International Journal of Solids and Structures 274 (2023) 112293

Contents lists available at ScienceDirect

International Journal of Solids and Structures

journal homepage: www.elsevier.com/locate/ijsolstr

Frictional shakedown of a coupled continuous contact

N. Cwiekala [a,*], J.R. Barber [b], D.A. Hills [a]

[a] Department of Engineering Science, University of Oxford, Parks Road, OX1 3PJ Oxford, United Kingdom
[b] Department of Mechanical Engineering, University of Michigan, Ann Arbor, MI 48109-2125, USA

ARTICLE INFO

Keywords:
Shakedown
Coupled contact
Partial slip
History dependence
Melan's theorem

ABSTRACT

The plane elastic problem of a circular disc shrink fitted into a hole in an elastically similar plane, with a frictional interface, is studied. The disc is subject to a radial force and torque both of which vary with time. In the steady-state the loads vary harmonically, and a relative phase shift is considered. Frictional slip is accounted for by edge dislocations distributed along the interface. It is shown that the steady-state response, which might, for example, be cyclic slip or full adhesion (shakedown) for a particular loading regime, depends on the loading history before the steady-state loading regime is entered. This contrasts with Melan's theorem for elastic–plastic shakedown, and is a consequence of the normal–tangential coupling in this frictional system.

1. Introduction

Contacts in mechanical assemblies are often subject to a constant primary load such as the centrifugal force in a gas turbine, and a superimposed varying load that might stem from vibration. These loads can cause regions of microslip to develop at the interface of a nominally stationary contact. The contact is then said to be in a state of partial slip. In the steady state, we distinguish between 'cyclic slip', where the slip displacements are fully reversed in each loading cycle, and 'ratchetting' where an increment of rigid-body motion is accumulated in each cycle, even though there is no instant in time at which the whole contact slips. Examples of frictional ratchetting include a punch 'walking' along a half-plane (Mugadu et al., 2004) and the gradual rotation of a bushing in a conrod end (Antoni et al., 2007).

1.1. Shakedown

In some circumstances, microslip during an initial transient phase can generate residual tractions sufficient to inhibit microslip in the steady state. This is analogous to the state of shakedown in an elastic–plastic system, and for many years tribologists assumed that Melan's theorem (Melan, 1936) could be extended to frictional slip, implying that shakedown will always occur if there exists a distribution of slip-generated residual tractions sufficient to inhibit slip. However, Klarbring et al. (2007) showed that this is true if and only if the system is 'uncoupled', meaning that slip displacements have no effect on the normal tractions at any point on the contact interface. A more general result due to Andersson et al. (2014) showed that for uncoupled systems above the shakedown limit, the frictional energy dissipation per cycle is also independent of initial conditions. However, when the system is coupled, we can expect a range of loading conditions in which the occurrence of shakedown depends on the initial condition or on an initial transient loading phase.

1.2. Load factor concept

The Coulomb friction law predicts that slip depends only on the ratio between the tangential and normal tractions, so we should expect that the occurrence of shakedown depends on an appropriate dimensionless measure λ of the ratio between the periodic load and the constant load. For coupled systems, we then anticipate the existence of a finite range $\lambda_1 < \lambda < \lambda_2$ in which the occurrence of shakedown depends on initial conditions, with shakedown always occurring for $\lambda < \lambda_1$. Jang and Barber (2011b) identified an additional range $\lambda_2 < \lambda < \lambda_3$ in which cyclic slip occurs in the steady state, but the energy dissipated per cycle depends on initial conditions. This implies that the system has 'memory', which Barber (2011) argued must reside in the locked-in slip displacements at points that do not slip in the steady state. Thus, the upper limit λ_3 is defined by the condition that all points in the interface slip at least once during each loading cycle. For systems possessing a rigid-body motion degree of freedom this may lead to ratchetting in $\lambda > \lambda_3$.

The complexity of most frictional engineering contact problems does not allow for an analytical solution, and hence illustrations of these concepts have been largely restricted to discrete formulations such as the finite element description of a complete contact due to like Flicek et al. (2015). Also, classical half-space contact geometries are either

* Corresponding author.
E-mail address: nils.cwiekala@eng.ox.ac.uk (N. Cwiekala).

https://doi.org/10.1016/j.ijsolstr.2023.112293
Received 2 February 2023; Received in revised form 23 April 2023; Accepted 25 April 2023
Available online 30 April 2023

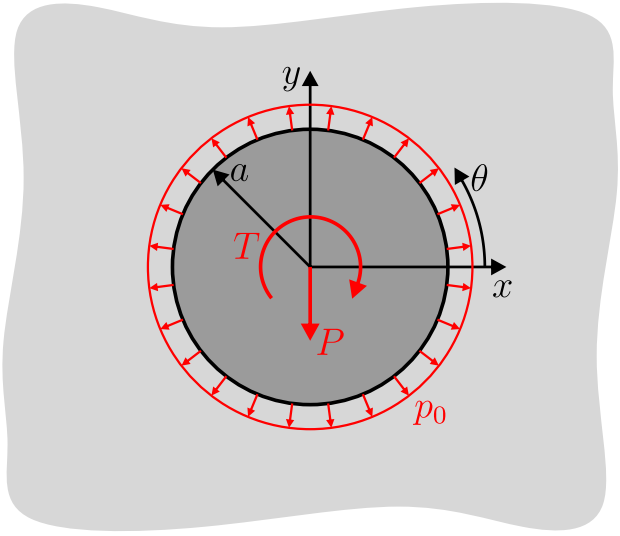

Fig. 1. Shrink-fitted disc in an infinite plane with a hole.

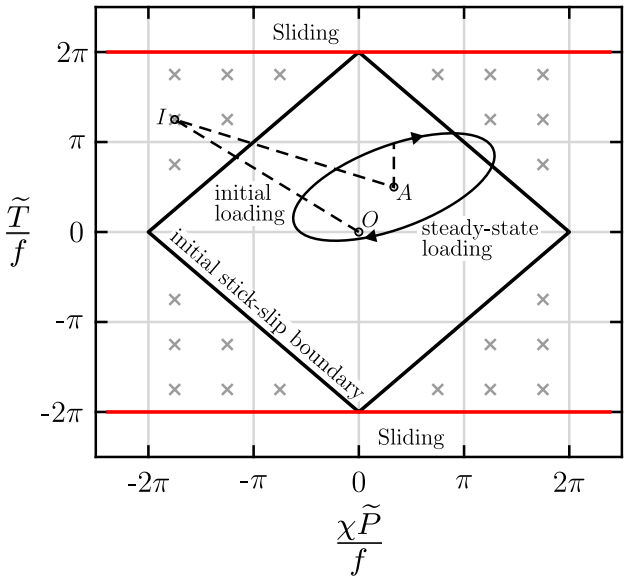

Fig. 2. Cyclic variation of radial load and torque in normalised load space.

uncoupled or have relatively weak normal-tangential coupling. In the present paper, we choose a simple circular geometry that lends itself to analytical formulation and that involves strong coupling, so as to highlight the effect of initial conditions on steady-state behaviour.

2. Problem statement

We consider the problem of Fig. 1 in which a disc of radius a is shrink-fitted into a circular hole in an infinite plate of the same material, resulting in a uniform interfacial contact pressure p_0.

The disc is then subject to a radial force P and a torque T applied at the origin in the sense shown in Fig. 1. In the absence of slip, these loads cause contact tractions of the form

$$p(\theta) = -\sigma_{rr}(a,\theta) = p_0 - \frac{\kappa+3}{\kappa+1}\frac{P}{2\pi a}\sin\theta \tag{1}$$

$$q(\theta) = -\sigma_{r\theta}(a,\theta) = -\frac{T}{2\pi a^2} - \frac{\kappa-1}{\kappa+1}\frac{P}{2\pi a}\cos\theta \tag{2}$$

where

$$\kappa = \begin{cases} 3-4\nu & \text{for plane strain,} \\ \frac{3-\nu}{1+\nu} & \text{for plane stress,} \end{cases}$$

is Kolosov's constant and ν is Poisson's ratio.

Starting from the uniform pressure state at $P = T = 0$, the contact interface will remain fully stuck as long as the normalised loads

$$\widetilde{P} = \frac{P}{p_0 a}\ ;\quad \widetilde{T} = \frac{T}{p_0 a^2} \tag{3}$$

remain inside the square region in Fig. 2, where

$$\chi = \sqrt{\left(\frac{\kappa-1}{\kappa+1}\right)^2 + f^2\left(\frac{\kappa+3}{\kappa+1}\right)^2} \tag{4}$$

(Cwiekala et al., 2022).

If the loading point crosses the boundary of this region, parts of the contact interface will experience slip. Cwiekala et al. (2022) represented the resulting stress field using arrays of distributed edge dislocations $B_r(\phi), B_\theta(\phi)$ at the interface, and used the resulting solution to investigate the range of 'memory-free' loading conditions under which the stress state depends only on the instantaneous values of $\widetilde{P}, \widetilde{T}$. Here we shall use the same methodology to investigate history-dependent loading scenarios, particularly those involving periodic loading.

2.1. Locked-in slip displacements

The system memory resides in the locked-in slip displacements $h(\theta) = u_\theta(a^+,\theta) - u_\theta(a^-,\theta)$, which in turn are completely defined by the instantaneous dislocation distributions $B_r(\phi), B_\theta(\phi)$. The tractions ((1), (2)) are then modified by the addition of the residual tractions

$$\bar{p}(\theta) = \frac{2\mu}{\pi(\kappa+1)}\int_S \left[B_\theta(\phi)K_{p\theta}(\theta,\phi) + B_r(\phi)K_{pr}(\theta,\phi)\right]d\phi \tag{5}$$

$$\bar{q}(\theta) = \frac{2\mu}{\pi(\kappa+1)}\int_S \left[B_\theta(\phi)K_{q\theta}(\theta,\phi) + B_r(\phi)K_{qr}(\theta,\phi)\right]d\phi\,, \tag{6}$$

where S defines the region in which slip has occurred and

$$\begin{aligned} K_{p\theta}(\theta,\phi) &= \frac{1}{2}\cos(\theta-\phi) + 1 \\ K_{q\theta}(\theta,\phi) = K_{pr}(\theta,\phi) &= \frac{\sin(\theta-\phi)\cos(\theta-\phi)}{2(1-\cos(\theta-\phi))} \\ K_{qr}(\theta,\phi) &= -\frac{1}{2}\cos(\theta-\phi)\ . \end{aligned} \tag{7}$$

Assuming $B_r(\phi), B_\theta(\phi)$ are known at the start of a given loading step, the values at the end of the same step can be found by solving an incremental contact problem in which the *incremental* dislocation distributions $\Delta B_r(\phi), \Delta B_\theta(\phi)$ are zero in the stick region where $|q(\theta)| < f\,p(\theta)$, and $q(\theta) = \pm f\,p(\theta)$ in the current slip region $\eta_1 < \theta < \eta_2$. This condition leads to the singular integral equation

$$\begin{aligned} &\int_{\eta_1}^{\eta_2}\left[\Delta B_\theta(\phi)\left(K_{q\theta} \mp f K_{p\theta}\right) + \Delta B_r(\phi)\left(K_{qr} \mp f K_{pr}\right)\right]d\phi \\ &\qquad = -\left(q_0(\theta) + \bar{q}(\theta)\right) \pm f\left(p_0(\theta) + \bar{p}(\theta)\right)\ ;\quad \eta_1 < \theta < \eta_2\,, \end{aligned} \tag{8}$$

where $p_0(\theta), q_0(\theta)$ represent the biaxial tractions of Eqs. (1), (2) and the condition that there be no separation requires that

$$B_\theta + \frac{dB_r}{d\phi} = 0\,. \tag{9}$$

The incremental problem (8) was solved numerically at each time step, using the procedure described in Cwiekala et al. (2022). The dislocation distributions were then updated and the process repeated. Notice however that if the incremental problem involves a transition at any point from slip to stick (a state known as 'advancing stick'), the load increment must be sufficiently small to capture the profile of the newly locked-in dislocation distributions.

2.2. Initial conditions

Generally, the steady-state cyclic dissipation is expected to depend on initial conditions, as described in Section 1. For example scenarios, these can be realised by defining a non-zero initial dislocation distribution, taking care that this does not lead to tractions that violate the frictional condition $|q(\theta)| \leq fp(\theta)$ for all θ. However, a more convenient method which we use here is to define various initial transient loading paths and use the present solution algorithm to determine the corresponding dislocation distributions.

If the steady-state cycle contains a segment that lies inside the square 'initial stick' region in Fig. 2, and if the initial transient load path is totally included inside this region, it is clear that the resulting steady state cycle must be unique. Thus to generate a range of different solutions corresponding to the same steady-state loading cycle, the initial loading paths must pass outside the initial stick region. For this purpose, we defined a set of trajectories of the form OIA in Fig. 2, where the points $\{\chi\widetilde{P}_I/f, \widetilde{T}_I/f\}$ comprise the 24 crosses in Fig. 2 whose coordinates are defined by various combinations of $\pm 3\pi/4, \pm 5\pi/4, \pm 7\pi/4$. We also included the 'full stick' transient OA.

This choice of initial transients is arbitrary and by no means comprehensive, but as we shall see it suffices to demonstrate various significant features of the steady-state response.

2.3. Steady-state loading

We assume that the steady-state loading can be expressed in the form

$$\begin{aligned} P(t) &= P_0 + P_1 \sin(\omega t) \\ T(t) &= T_0 + T_1 \sin(\omega t + \varphi)\,, \end{aligned} \tag{10}$$

where P_0, T_0 are the mean loads, P_1, T_1 are the amplitudes of the periodic loads [e.g. due to vibration] and t is time. If the periodic loads are in phase ($\varphi = 0$), the steady-state load path collapses to a straight line in Fig. 2. For all other cases, Eqs. (10) define an elliptical load path centred on the point $\{\chi\widetilde{P}_0/f, \widetilde{T}_0/f\}$.

In the spirit of Section 1.2, we write Eqs. (10) in the dimensionless form

$$\frac{1}{f}\begin{bmatrix}\chi\widetilde{P}(t)\\ \widetilde{T}(t)\end{bmatrix} = \frac{1}{f}\begin{bmatrix}\chi\widetilde{P}_0\\ \widetilde{T}_0\end{bmatrix} + \frac{\lambda}{\sqrt{1+\psi^2}}\begin{bmatrix}\sin(\omega t)\\ \psi\sin(\omega t+\varphi)\end{bmatrix}\,. \tag{11}$$

where

$$\lambda = \frac{1}{f}\sqrt{\left(\chi\widetilde{P}_1\right)^2 + \left(\widetilde{T}_1\right)^2}\,, \tag{12}$$

is a dimensionless load factor, and

$$\psi = \frac{\widetilde{T}_1}{\chi\widetilde{P}_1}\,. \tag{13}$$

In the special case where $\varphi = 0$, λ is half the length of the line defining the load path in Fig. 2 and ψ is its slope.

2.4. Steady-state response

We choose to characterise the steady-state response in terms of the total energy dissipated per load cycle, since this is likely to correlate with the severity of fretting damage, and it provides a convenient scalar measure of the extent to which initial conditions influence the steady-state.

The instantaneous rate of energy dissipation due to friction is given by

$$\dot{W} = -a\int_0^{2\pi} q(\theta)\dot{h}(\theta)d\theta\,, \tag{14}$$

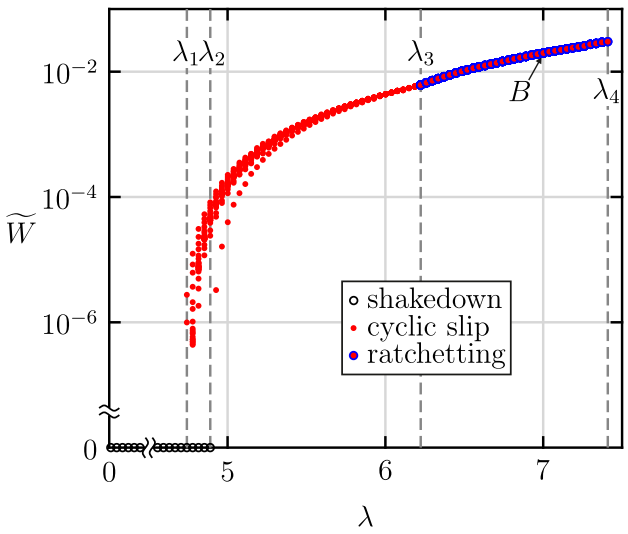

Fig. 3. Normalised steady-state energy dissipation per cycle $\widetilde{W}$ as a function of load factor λ for in-phase loading with $\chi\widetilde{P}_0/f = \pi, \widetilde{T}_0/f = 3\pi/4, \psi = 5/8$ and $f = 0.1$. Results are presented for all 25 initial loading conditions defined in Section 2.2 (plane strain with $\nu = 0.3$).

where $\dot{h}(\theta)$ is the instantaneous rate of local slip displacement which is non-zero only in the current slip zone. The cyclic dissipation is then obtained as

$$W = \int_{\text{cycle}} \dot{W}\,dt\,, \tag{15}$$

and a convenient normalisation is

$$\widetilde{W} = \frac{W\mu}{(\kappa+1)p_0^2 a^2}\,. \tag{16}$$

In some cases we found that the system approaches the steady state asymptotically, as in the problem considered by Ahn and Barber (2008). In these cases, the steady state was considered converged when the change in $\widetilde{W}$ relative to the previous cycle was less that 0.01%.

3. In-phase loading

When the periodic loads are in phase ($\varphi = 0$), the load path in Fig. 2 is a straight line and we expect the bounding load factors $\lambda_1, \ldots, \lambda_4$ described in Section 1.2 to depend on the slope of this line ψ and the mean values $\chi\widetilde{P}_0/f, \widetilde{T}_0/f$. Fig. 3 shows the normalised steady-state energy dissipation per cycle for 25 different initial transients, for the case where $\chi\widetilde{P}_0/f = \pi, \widetilde{T}_0/f = 3\pi/4$ and $\psi = 5/8$. Shakedown cases are represented by black circles, cyclic slip by red dots, and ratchetting by red dots with a blue edge. The results follow the pattern described in Section 1.2, notably that there exists a range of load factors $\lambda_1 < \lambda < \lambda_2$ in which the occurrence of shakedown depends on initial conditions, and that the energy dissipation is non-zero but dependent on initial conditions in the range $\lambda_2 < \lambda < \lambda_3$. Ratchetting occurs for $\lambda > \lambda_3$ and gross slip (unbounded rigid-body rotation) at one point in the cycle for a higher value of λ which we identify as λ_4.

The limiting value λ_2 can be regarded as the solution of an optimisation problem in which we seek a distribution of locked-in slip displacements $h(\theta)$ so as to just inhibit slip throughout the loading cycle. For in-phase loading it is sufficient to apply this condition at the two extreme conditions represented by the ends of the load line. For this purpose, the continuum problem was first converted to a discrete problem by discretising $h(\theta)$, after which the optimal distribution was obtained using the procedure described by Björkman and Klarbring (1987) and Flicek et al. (2015).

This procedure was used to determine the boundary λ_2 shown in Fig. 3. The optimal distribution was considered as an additional initial

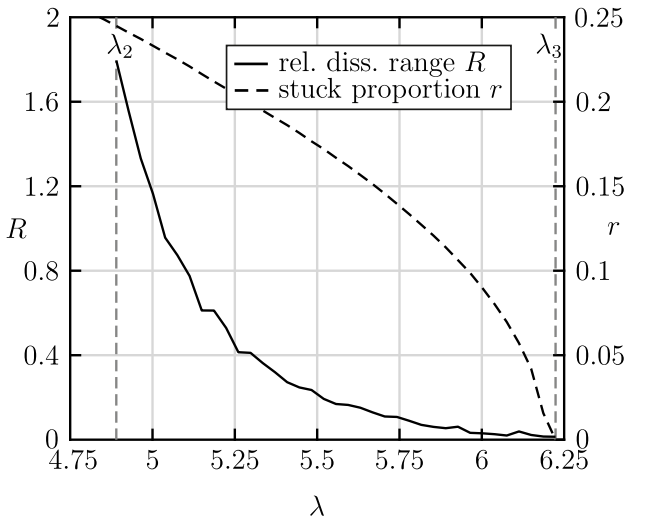

Fig. 4. Relative range of energy dissipation R [Eq. (17)] for $\lambda_2 < \lambda < \lambda_3$ and the parameters of Fig. 3, compared with the fraction r of the interface that remains stuck after the initial loading phase OIA in Fig. 2.

condition and the corresponding values of steady-state dissipation comprise the outlying rightmost red dots in the range $\lambda_2 < \lambda < \lambda_3$. These points lie significantly to the right of all those obtained using the 24 initial conditions defined in Section 2.2, which shows that this choice of initial conditions was not sufficiently comprehensive to capture the full range of history-dependent behaviour, both in regard to the possibility of shakedown in $\lambda < \lambda_2$ and to the expected value of energy dissipation in $\lambda_2 < \lambda < \lambda_3$. However, it remains an open question as to whether there exists any transient loading path from the initial axisymmetric state, sufficient to generate the optimal slip displacements. A related problem for a simple frictional contact was considered by Barber (2018) who showed that a desired distribution of residual stress in a one-dimensional discrete system could be achieved by a finite sequence of alternating loads of monotonically decreasing amplitude, but that for the corresponding continuous system the desired value could generally only be attained at a denumerable set of points.

3.1. System memory

We anticipate that memory of the initial conditions resides primarily in regions that slipped during the initial transient loading phase, OIA in Fig. 2 and that subsequently remained permanently stuck. To confirm this, Fig. 4 presents the proportion r of these regions that remains stuck after point A in Fig. 2, and compares it with the relative range of energy dissipation

$$R = \frac{\max(\widetilde{W}) - \min(\widetilde{W})}{\mathrm{mean}(\widetilde{W})}, \tag{17}$$

As expected, both measures tend monotonically to zero as λ_3 is approached, since in ratchetting all points in the contact area slip at least once per cycle and all memory of the initial conditions must eventually be lost.

3.2. Ratchetting

Fig. 5 shows the time history of regions of forward and backward slip for $\lambda = 7$, corresponding to the point B in Fig. 3.

All the other parameters are the same as in Fig. 3. Notice that some regions experience just a single period of forward slip during each load cycle, whilst others experience alternating periods of forward and backward slip. We describe this as *non-monotonic ratchetting*. Of course, kinematic considerations dictate that the net slip displacement per cycle be the same for all points in the interface.

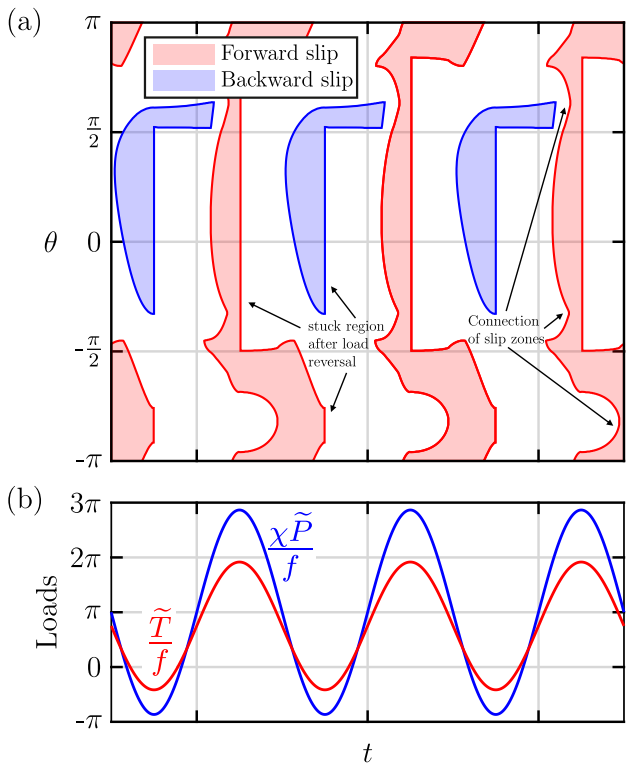

Fig. 5. (a) Evolution of slip zones around the circumference for ratchetting with parameters corresponding to point B in Fig. 3, (b) the corresponding load variation.

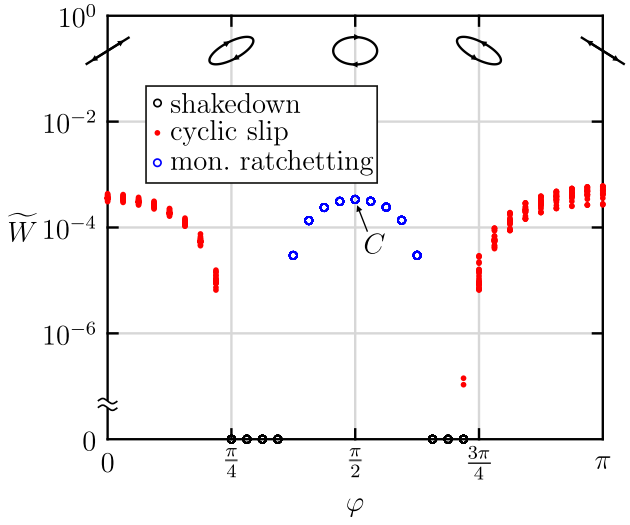

Fig. 6. Normalised steady-state energy dissipation per cycle $\widetilde{W}$ as a function of relative phase φ for $\chi\widetilde{P}_0/f = \pi, \widetilde{T}_0/f = 3\pi/4, \psi = 5/8, \lambda = 5.1$ and $f = 0.1$. Results are presented for all 25 initial loading conditions defined in Section 2.2 (plane strain with $\nu = 0.3$).

4. Out-of-phase loading

Jang and Barber (2011a) and Kim et al. (2019) describe results for frictional systems in which the relative phase of the periodic loads has a significant effect on the frictional energy dissipation. For the present system, the case $\varphi \neq 0$ corresponds to an elliptical path in Fig. 2. Fig. 6 shows the dimensionless cyclic energy dissipation $\widetilde{W}$ as a function of φ for the case $\chi\widetilde{P}_0/f = \pi, \widetilde{T}_0/f = 3\pi/4, \psi = 5/8$ and $\lambda = 5.1$, for the 25 initial conditions defined in Fig. 2 and Section 2.2.

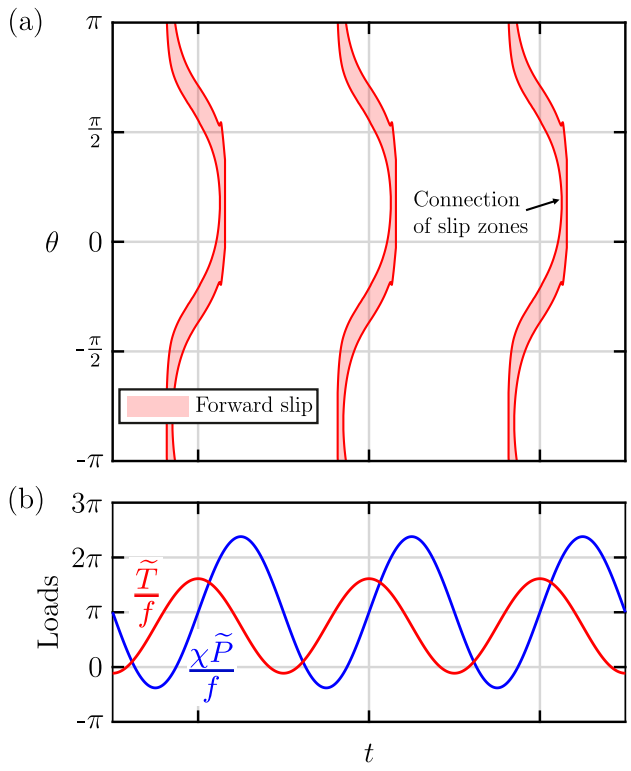

Fig. 7. (a) Evolution of slip zones around the circumference for ratchetting with parameters corresponding to point C in Fig. 6, (b) the corresponding load variation.

Notice that changing only the relative phase of the oscillating torque and force has a qualitative effect on the steady-state response, with ranges of cyclic slip, shakedown and ratchetting. As in the in-phase case, the initial conditions influence the location of the boundary between shakedown and cyclic slip and also the energy dissipation in cases of cyclic slip.

4.1. Monotonic ratchetting

Fig. 7 shows the extent of the slip region for a representative point C in the ratchetting range of Fig. 6. In each load cycle a single slip zone forms near $\theta = -3\pi/4$, after which it bifurcates into two separate slip zones. These slip zones then move away from each other around the circumference, until they merge again near $\theta = \pi/4$. In contrast to Fig. 5, no points experience slip opposite to the ratchetting direction, so we refer to this steady state as *monotonic ractchetting*.

4.2. Memory-free steady states

Fig. 8 shows the steady-state dissipation and the corresponding state as a function of the load factor λ for $\varphi = \pi/2$ and the same parameters as in Fig. 6 ($\chi\widetilde{P}_0/f = \pi, \widetilde{T}_0/f = 3\pi/4, \psi = 5/8$).

Notice that there is a sharp transition from shakedown to monotonic ratchetting (blue circles) at $\lambda = 5$ (so $\lambda_1 = \lambda_2 = \lambda_3$), and that the dissipation is independent of initial conditions for all λ. However, for $\lambda > 6.3$, the behaviour transitions to non-monotonic ratchetting, as defined in Section 3.2, here identified by blue circles with a red dot.

4.3. Effect of load factor

Fig. 9 shows the effect of a relative phase φ on the steady-state dissipation for a range of load factors.

Here, in contrast to Figs. 3, 6 and 8, we consider only the direct path OA to the load cycle. If other initial conditions were included,

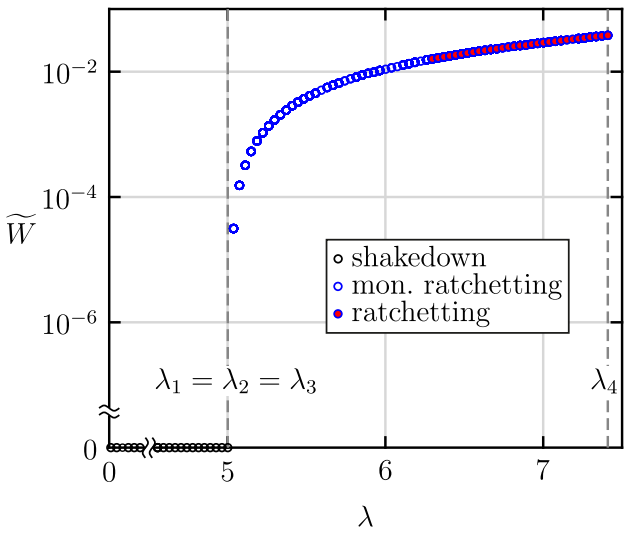

Fig. 8. Normalised steady-state energy dissipation per cycle $\widetilde{W}$ as a function of load factor λ for out-of-phase loading ($\varphi = \pi/2$) with $\chi\widetilde{P}_0/f = \pi, \widetilde{T}_0/f = 3\pi/4, \psi = 5/8$ and $f = 0.1$. Results are the same for all the 25 initial loading conditions defined in Section 2.2 (plane strain with $\nu = 0.3$).

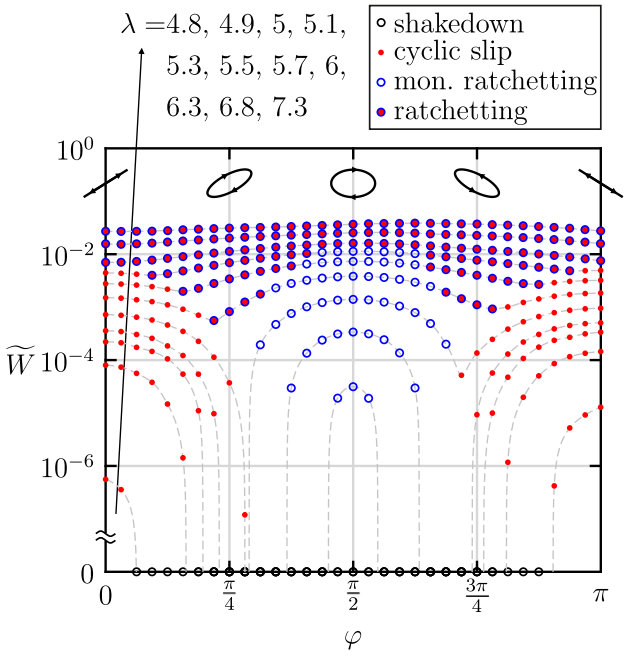

Fig. 9. Normalised steady-state energy dissipation per cycle $\widetilde{W}$ as a function of relative phase φ for $\chi\widetilde{P}_0/f = \pi, \widetilde{T}_0/f = 3\pi/4, \psi = 5/8, f = 0.1$ and a range of load factors λ. The initial transient is defined by a straight line from O to A in Fig. 2 (plane strain with $\nu = 0.3$).

the cyclic slip data points (red dots) would show some variability, but the ratchetting results would remain unchanged. By tracking the dissipation and state along a vertical line near $\varphi = 0$ or near $\varphi = \pi/2$ it is clear that figures similar to Fig. 3 and Fig. 6 respectively would be obtained.

5. Conclusion

The steady-state frictional energy dissipation at the contact interface generally increases if the load factor λ characterising the severity of the periodic loading is increased. Depending on the parameter values including the relative phase of the periodic force and torque, the

following sequences of the steady-state mode can occur with increasing λ

1. Shakedown → cyclic slip → non-monotonic ratchetting,
2. Shakedown → monotonic ratchetting → non-monotonic ratchetting,

and the sequence can always be cut short by sliding or separation. Only for load cases exhibiting the first sequence do we find a conditional shakedown region $\lambda_1 < \lambda < \lambda_2$, as shown in Fig. 3, and we then also find that the frictional energy dissipation during cyclic slip depends on initial conditions.

Declaration of competing interest

The authors declare the following financial interests/personal relationships which may be considered as potential competing interests: Nils Cwiekala reports financial support was provided by Rolls-Royce plc. David Hills reports financial support was provided by Rolls-Royce plc.

Data availability

No data was used for the research described in the article.

Acknowledgements

N. Cwiekala and D.A. Hills thank Rolls-Royce plc and the EPSRC for the support under the Prosperity Partnership Grant 'Cornerstone: Mechanical Engineering Science to Enable Aero Propulsion Futures', Grant Ref: EP/R004951/1.

References

Ahn, Y.J., Barber, J.R., 2008. Response of frictional receding contact problems to cyclic loading. Int. J. Mech. Sci. 50 (10–11), 1519–1525.

Andersson, L.-E., Barber, J., Ponter, A., 2014. Existence and uniqueness of attractors in frictional systems with uncoupled tangential displacements and normal tractions. Int. J. Solids Struct. 51 (21–22), 3710–3714.

Antoni, N., Nguyen, Q.-S., Ligier, J.-L., Saffré, P., Pastor, J., 2007. On the cumulative microslip phenomenon. Eur. J. Mech. A Solids 26 (4), 626–646.

Barber, J.R., 2011. Frictional systems subjected to oscillating loads. Ann. Solid Struct. Mech. 2 (2–4), 45–55.

Barber, J.R., 2018. Contact Mechanics. Springer.

Björkman, G., Klarbring, A., 1987. Shakedown and residual stresses in frictional systems. In: Contact Mechanics and Wear of Rail/Wheel Systems II: Proceedings of the 2nd International Symposium. University of Waterloo Press, pp. 27–39.

Cwiekala, N., Barber, J.R., Hills, D.A., 2022. Memory-free loading paths for a coupled continuous contact problem with friction. Mech. Res. Commun. 124, 103958.

Flicek, R., Hills, D., Barber, J., Dini, D., 2015. Determination of the shakedown limit for large, discrete frictional systems. Eur. J. Mech. A Solids 49, 242–250.

Jang, Y.H., Barber, J., 2011a. Effect of phase on the frictional dissipation in systems subjected to harmonically varying loads. Eur. J. Mech. A Solids 30 (3), 269–274.

Jang, Y.H., Barber, J., 2011b. Frictional energy dissipation in materials containing cracks. J. Mech. Phys. Solids 59 (3), 583–594.

Kim, S., Ahn, Y.J., Jang, Y.H., 2019. Frictional energy dissipation for coupled systems subjected to harmonically varying loads. Tribol. Int. 134, 205–210.

Klarbring, A., Ciavarella, M., Barber, J., 2007. Shakedown in elastic contact problems with Coulomb friction. Int. J. Solids Struct. 44 (25–26), 8355–8365.

Melan, E., 1936. Theorie statisch unbestimmter systeme aus ideal-plastichem baustoff. Sitzungsber. d. Akad. d. Wiss. 145, 195–218.

Mugadu, A., Sackfield, A., Hills, D., 2004. Analysis of a rocking and walking punch—Part I: initial transient and steady state. J. Appl. Mech. 71 (2), 225–233.